Electronic Supporting Information (ESI)

Laser Doping of 2D Material for Precise Energy Band Design

Xiang Tan[1,2,†], Shu Wang[1,†], Qiaoxuan Zhang[3,†], Juxing He[1], Shengyao Chen[1,5], Yusong Qu[1], Zhenzhou Liu1,6, Yong Tang[3], Xintong Liu[3], Cong Wang[4]*, Quan Wang[2]* and Qian Liu[1,5]*

[1] CAS Center for Excellence in Nanoscience, National Center for Nanoscience and Technology & University of Chinese Academy of Sciences, Beijing 100190, China

[2] Zhenjiang key laboratory of advanced sensing materials and devices, School of Mechanical Engineering, Jiangsu University, Zhenjiang 212013, P.R. China

[3] Hebei University of Water Resources and Electric Engineering Electrical Automation Department, 061001, Cangzhou, Hebei, China

[4] College of Mathematics and Physics, Beijing University of Chemical Technology, Beijing, 100029, China

[5] MOE Key Laboratory of Weak-Light Nonlinear Photonics, TEDA Applied Physics Institute, School of Physics, Nankai University, Tianjin 300457, China

[6] School of Physical Science and Technology ,Inner Mongolia University, Inner Mongolia 010000,China

Section 1. Characterization of $MoTe_2$

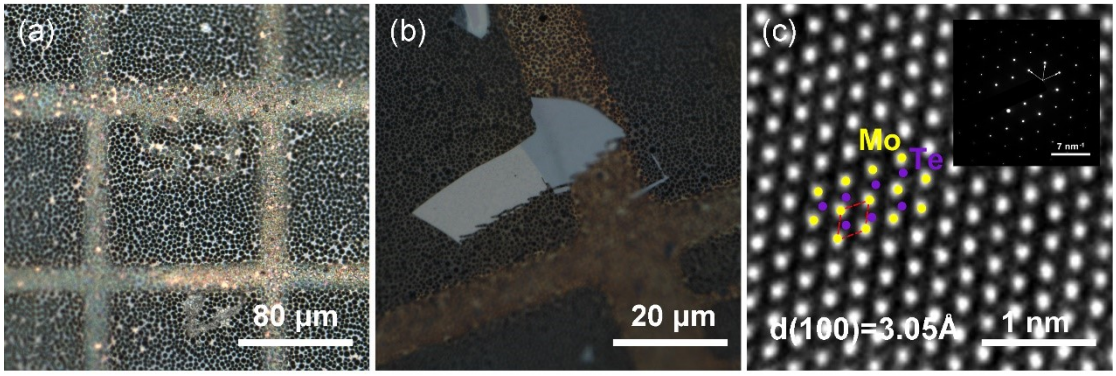

Fig. S1. (a) Optical image of microgrid copper mesh. **(b)** Optical image of $MoTe_2$ transferred to a copper grid by wet process. **(c)** TEM image of $MoTe_2$.

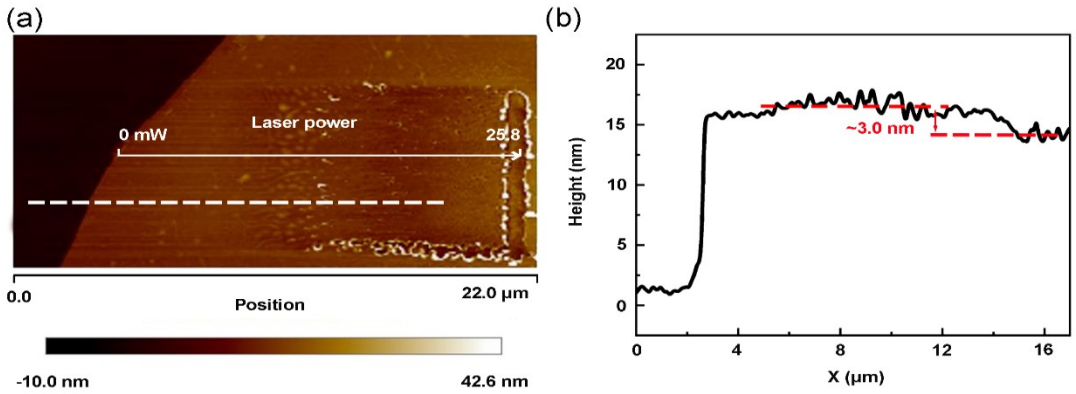

Fig. S2. (a, b) AFM image of $MoTe_2$ after power gradient laser irradiation, the curve in **(b)** corresponds to $MoTe_2$ at the white dashed line, where the laser power ranges from 0 mW to 25.8 mW, and the laser pulse width is kept at 2000 ns.

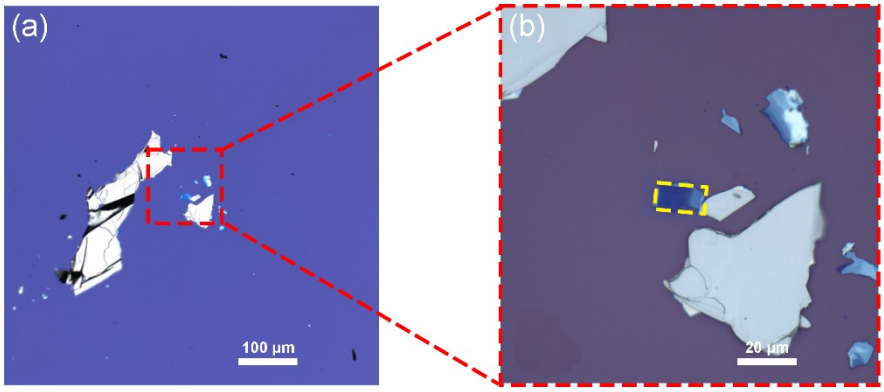

Fig. S3. (a, b) Optical image of $MoTe_2$ after power gradient laser irradiation, the area in the yellow box is the laser irradiation area, where the laser power ranges from 0 mW to 25.8 mW, and the laser pulse width is kept at 2000 ns.

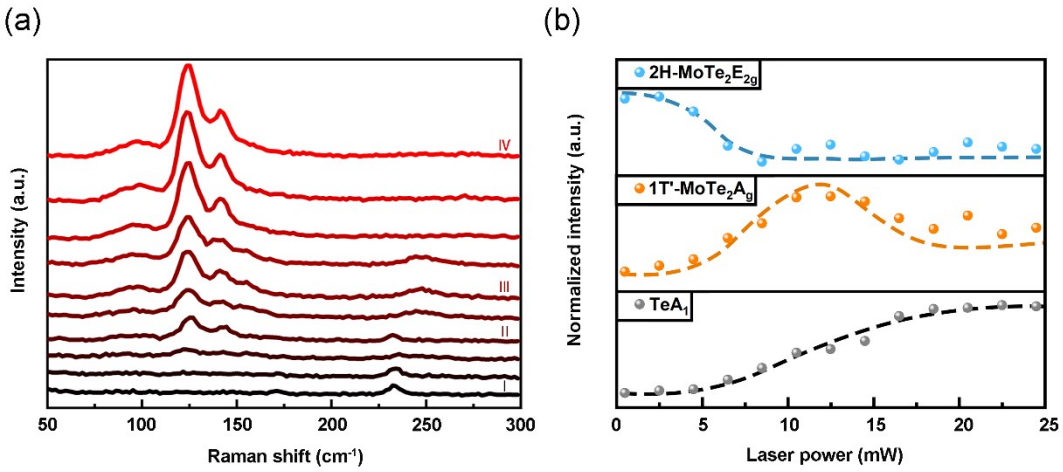

Fig. S4. (a) Raman measurement of $MoTe_2$ after power gradient laser irradiation, the curves from bottom to top correspond to Raman spectrum after gradient laser action from 0 mw to 25.8 mw, where the sampling point spacing is the same. (b) Signal intensity at $MoTe_2$ and Te characteristic peak positions.

Section 2. The preparation process of the device and the electrical behavior of the device after laser irradiation

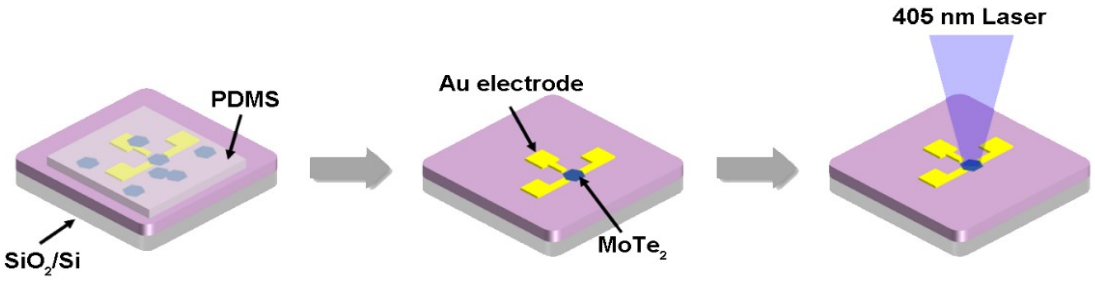

Fig. S5. Device preparation flow.

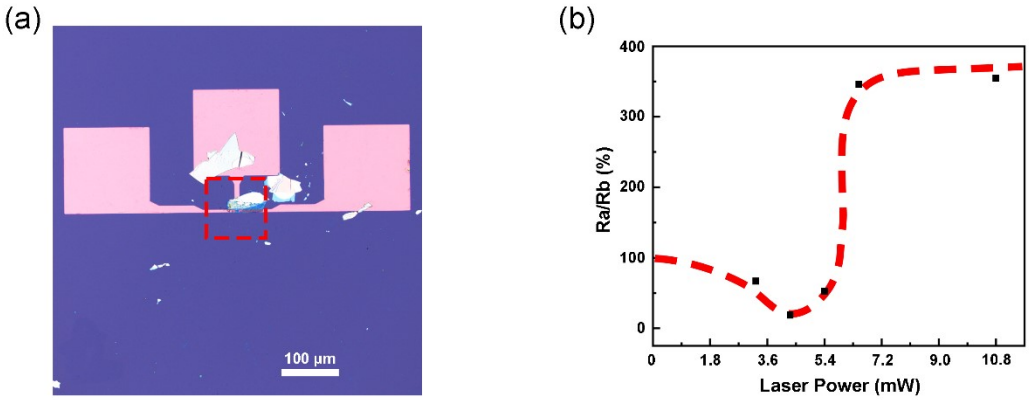

Fig. S6. (a) Optical image of a fully swept device. (b) The change in resistance of $MoTe_2$ after laser action, where Ra is the resistance of $MoTe_2$ after laser action and Rb is the original resistance of $MoTe_2$.

Because the doping we study is the result of laser-induced generation of molecular-vacancy clusters in the main lattice of 2H-$MoTe_2$, the doping level and distribution can be manipulated by varying the laser parameters. First, we performed laser power dependence measurements as shown in **Fig. S6a**, where $MoTe_2$ was transferred to a 5/25 nm Cr/Au bottom electrode with a 300 nm thick SiO_2 substrate. There was variability in the size and shape of the mechanically exfoliated $MoTe_2$, so it was scanned uniformly in the red boxed region of the figure. The laser pulse width is kept constant at 2000ns, and the laser power is adopted as 3.4mW, 4.4mW, 5.4mW, 6.4mW, 10.8mW. The resistance of the device after laser action changes as shown in **Fig. S6b**. Due to the strong electronegativity of oxygen, some electrons migrate out from $MoTe_2$ and the hole carriers become more, so when the laser power is less than 4.5mW, the device resistance obviously decreases, while when the laser power increases again, the sheet structure is destroyed and the device resistance becomes larger until it tends to a stable value.

Section 3. Temperature field simulation

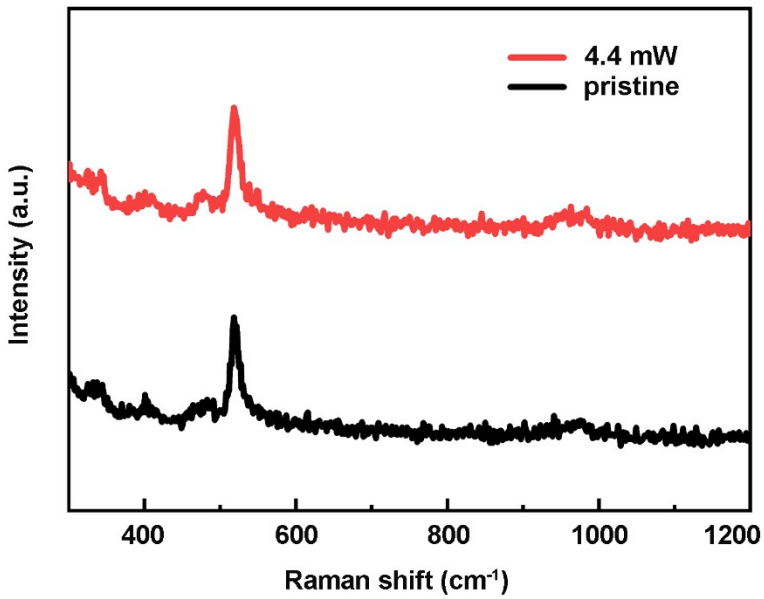

Fig. S7. Comparison of Raman of $MoTe_2$ after 4.4 mW laser action at wavelengths between 300 nm and 1200 nm and Raman of $MoTe_2$ without laser action, where the laser pulse width is 2000 ns.

Heat transfer simulation is performed by "COMSOL Multiphysics Software". The simulation object is 2H-$MoTe_2$ / SiO_2, where the thickness of $MoTe_2$ is 15 nm and the size is 10×10 μm. For mechanically exfoliated $MoTe_2$, $\rho = 157\times10^{-6}$ cm^3g^{-1}, $\lambda = 3$ $W\times m^{-1}\times K^{-1}$, C = 1.53 J/K/cm^3 (T = 280 K)[1,2]. According to the experiment, the ambient temperature and sample stage temperature are set to 300 K, the laser pulse time is 2000 ns, and the laser power is 4.4 mW. However, considering the light absorption rate of $MoTe_2$, the laser power of 0.8 mW is used in the simulation[3], and heat transfer model follows the heat transfer equation :

$$\rho C_p \frac{\partial T}{\partial t} + \rho C_p \mu \nabla T = \nabla \cdot (k \nabla T) + Q_v$$

Section 4. Total local density of states (LDOS) simulation

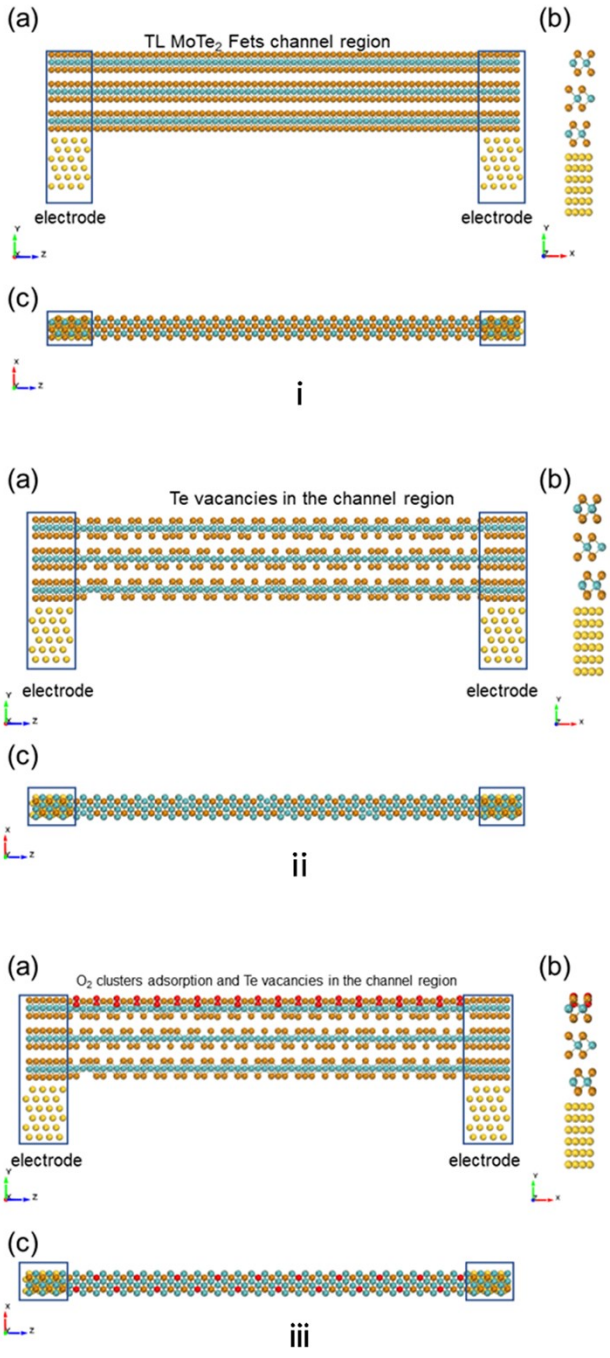

Fig. S8. Device Simulation Model. **i:**(a) Front and (b)side schematic models of TL $MoTe_2$ FETs with Au electrodes. (c) Top schematic model. ii**:** (a) Front and (b)side schematic models of TL $MoTe_2$ FETs with Te vacancies. (c) Top schematic model. **iii:** (a) Front and (b)side schematic models of TL $MoTe_2$ FET with O_2 clusters adsorption and Te vacancies. (c) Top schematic model.

The structural calculations were performed within the framework of density functional theory (DFT) using the Vienna ab-initio Simulation Package (VASP).[4] The wave functions were described in a plane wave basis set with an energy cutoff of 340~600 eV. The potentials

at the core region were treated with projector augmented wave (PAW) pseudopotentials.[5] We use vdW-DF level of optB86b exchange functional to consider the van der Waals interaction.[6] The Au/Three Layers(TL) $MoTe_2$ heterostructure is formed by vertically stacking A-B-C stacking 2H phase TL $MoTe_2$ to six layers Au, the interlayer distance is 3 Å between Au and $MoTe_2$. The Mo-Te and Au-Au bond lengths are 2.70 Å and 2.89 Å, respectively. The lattice parameter of TL $MoTe_2$ unite cell is 3.33 Å. The vacuum distances between the periodic cells are all kept to 50 Å. The geometry optimization was performed until the residual force fell below 0.001 eV/Å.

We calculated the transport properties by the the first-principles quantum transport package Nanodcal[7,8] using DFT coupled with nonequilibrium Green's function (NEGF) method.[9] A density mesh cutoff of 75 Hartree was applied. The temperature is 300 K. The transmission current I_d was expressed as:

$$Id(V_{ds},V_g)=\frac{2e}{h}\int_{-\infty}^{+\infty}\{T(E,V_{ds},V_g)[f_S(E-\mu_S)-f_D(E-\mu_D)]\}dE$$

where $T(E, V_{ds}, V_g)$ was transmission coefficient; f_S and f_D are Fermi-Dirac distribution function for the source and drain, respectively; and μ_S and μ_D are the electrochemical potential for the source and drain. The double-zeta polarized basis set (DZP)[10] was adopted. the exchange and correlation were at the level of the local density approximation (LDA)[11] in the in the PZ81 functional [10] was employed to calculated the exchange and correlation interaction. The Brillouin zone was sampled by the Monkhorst-Pack method with a sampled *k*-point mesh [12] with a separation of ~0.01 $Å^{-1}$. The system using a k-point mesh of 17×1×10 for the leads, the k-mesh was 17×1×1 for central region.

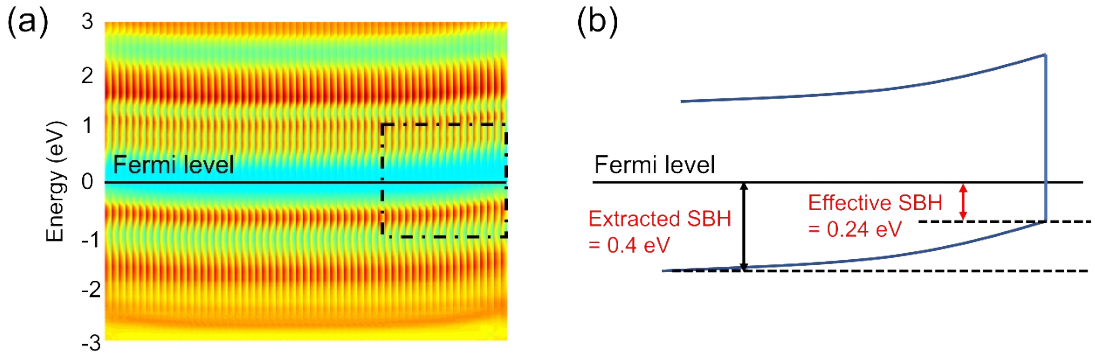

Fig. S9. Total local density of states (LDOS) of the channel region from (a) TL $MoTe_2$ FETs with Au electrodes. (b) is the extracted SBH schematic diagram of the framed part by a dashed line showed in **Fig. S9a**.

Section 5. Application of $MoTe_2$-based devices based on laser doping

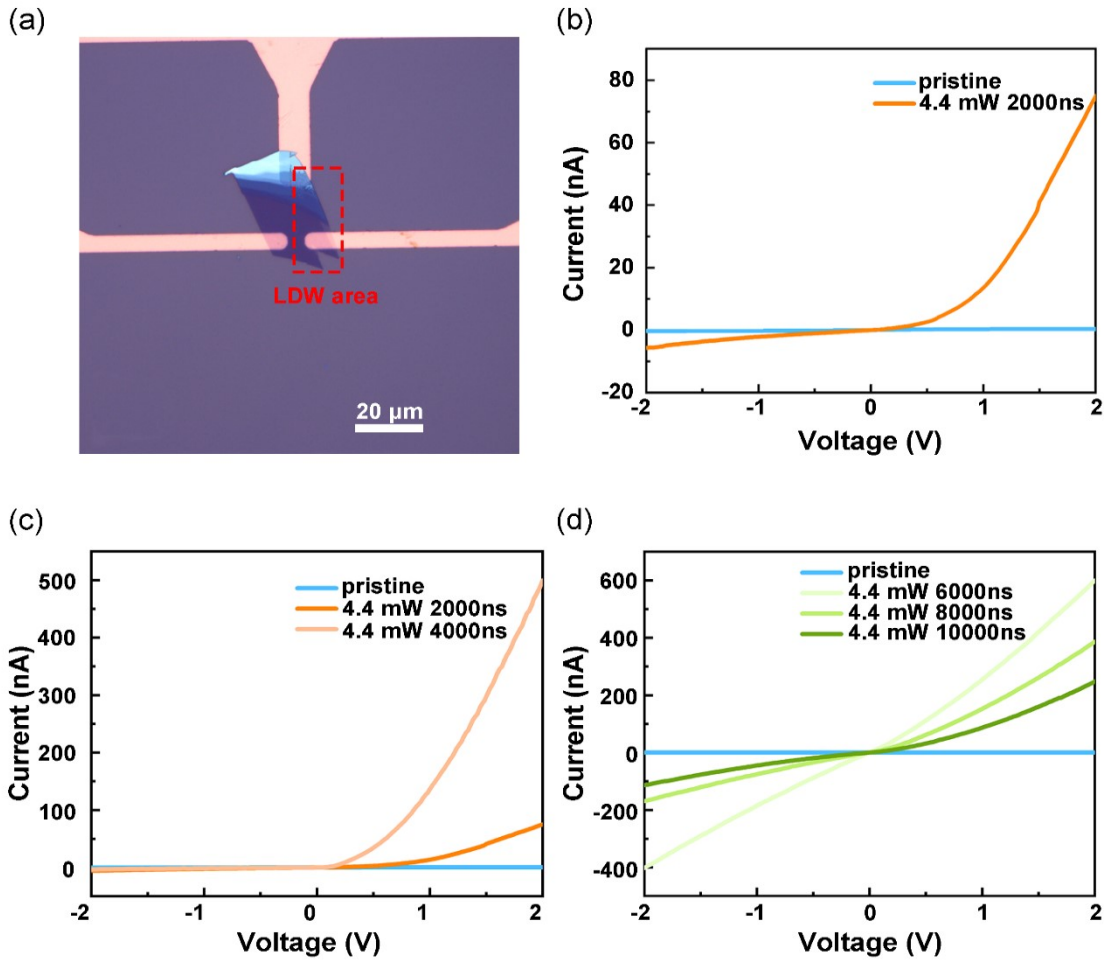

Fig. S10. (a) Optical image of a half-sweep device. (b,c,d) I-V curve of the device after multiple laser irradiation, where the laser irradiation area and laser parameters are constant each time.

We used a laser to inscribe $MoTe_2$, and the inscribed area is shown in the red box area in **Fig. S10a**, with laser parameters of 4.4 mW power and 2000 ns pulse width, and the device showed a rectification effect (**Fig. S10b**), which is a direct demonstration of the laser-induced pn junction. Afterwards, several laser irradiations were performed to regulate the rectification effect of the device, and the laser parameter settings were kept at 4.4 mW and 2000 ns. After the second irradiation, there was a significant increase in the rectification ratio of the device (**Fig. S10c**), which was due to the fact that the difference between the concentration of holes and electrons in the irradiated and unirradiated regions became larger. However, after multiple irradiations, the rectification effect of the device disappeared and even the conductivity deteriorated (**Fig. S10d**), indicating that even if the laser power is not high, too long an irradiation tim

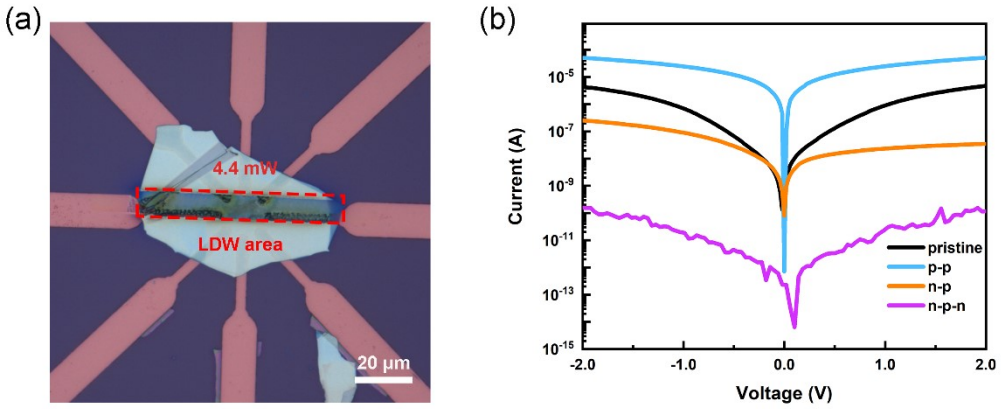

Fig. S11. (a) Optical image of a multifunctionally integrated device. (b) Electrical characteristics of the device.

References

[1] Chi Z, Chen H, Zhao Q*, et al*. Ultrafast carrier and phonon dynamics in few-layer 2H–MoTe2 [J]. *The Journal of Chemical Physics*, 2019, 151(11): 114704.

[2] Eisenmann B，Schäfer H. Sulfides, Selenides, Tellurides (Part 2) · MoReTe - NaSSb: Datasheet from Landolt-Börnstein - Group III Condensed Matter · Volume 14B2: "Sulfides, Selenides, Tellurides (Part 2)" in SpringerMaterials (https://doi.org/10.1007/10338439_20): Springer-Verlag Berlin Heidelberg.

[3] Seo S-Y, Park J, Park J*, et al*. Writing monolithic integrated circuits on a two-dimensional semiconductor with a scanning light probe [J]. *Nature Electronics*, 2018, 1(9): 512-517.

[4] Hafner J. Ab-Initio Simulations of Materials Using VASP: Density-Functional Theory and Beyond [J]. *J. Comput. Chem.*, 2008, 29(13): 2044−2078.

[5] Kresse G，Joubert D. From Ultrasoft Pseudopotentials to the Projector Augmented-Wave Method [J]. *Phys. Rev. B*, 1999, 59(3): 1758-1775.

[6] Klimeš J, Bowler D R，Michaelides A. Van der Waals Density Functionals Applied to Solids [J]. *Phys. Rev. B*, 2011, 83(19): 195131.

[7] Taylor J, Hong G，Jian W J P R B. Taylor, J., Guo, H. & Wang, J. Ab initio modeling of quantum transport properties of molecular electronic devices. Phys. Rev. B 63, 245407 [J]. 2001, 63(24).

[8] Waldron D, Haney P, Larade B*, et al*. Waldron, D., Haney, P., Larade, B., MacDonald, A. & Guo, H. Nonlinear spin current and magnetoresistance of molecular tunnel junctions. Phys. Rev. Lett. 96, 166804 (2006) [J]. 2006, 96(16): 166804.

[9] Datta S. Nanoscale Device Modeling: the Green's Function Method [J]. *Superlattices Microstruct.*, 2000, 28(4): 253−278.

[10] Sánchez-Portal D, Ordejón P, Artacho E*, et al*. Density-functional method for very large systems with LCAO basis sets [J]. 1997, 65(5): 453-461.

[11] Ramage D, Hall D, Nallapati R M*, et al*. Labeled LDA: a supervised topic model for credit attribution in multi-labeled corpora[C].Proceedings of the 2009 Conference on Empirical Methods in Natural Language Processing, EMNLP 2009, 6-7 August 2009, Singapore, A meeting of SIGDAT, a Special Interest Group of the ACL,2009.

[12] Monkhorst H J，Pack J D. Special Points for Brillouin-Zone Integrations [J]. *Phys. Rev. B*, 1976, 16(4): 1748−1749.